***J. Ocean Univ. China*** (Oceanic and Coastal Sea Research)
DOI 10.1007/s11802-014-2029-3
ISSN 1672-5182, 2014 13 (2): 1-10
*http://www.ouc.edu.cn/xbywb/*
*E-mail:xbywb@ouc.edu.cn*

# Application of CFD Modeling to Hydrodynamics of CycloBio Fluidized Sand Bed in Recirculating Aquaculture Systems

LIU Yao[1)], SONG Xiefa[1), *], LIANG Zhenlin[2)], and PENG Lei[1)]

1) *College of Fisheries*, *Ocean University of China*, *Qingdao* 266003, *P. R. China*
2) *College of Marine Science*, *Shandong University*, *Weihai* 264209, *P. R. China*

(Received May 3, 2012; revised June 27, 2012; accepted May 6, 2013)


**Abstract** To improve the efficiency of a CycloBio fluidized sand bed (CB FSB) in removal of dissolved wastes in recirculating aquaculture systems, the hydrodynamics of solid-liquid flow was investigated using computational fluid dynamics (CFD) modeling tools. The dynamic characteristics of silica sand within the CB FSB were determined using three-dimensional, unsteady-state simulations with the granular Eulerian multiphase approach and the RNG $k$-$\varepsilon$ turbulence model, and the simulation results were validated using available lab-scale measurements. The bed expansion of CB FSB increased with the increase in water inflow rate in numerical simulations. Upon validation, the simulation involving 0.55 mm particles, the Gidaspow correlation for drag coefficient model and the Syamlal-O'Brien correlation for kinetic granular viscosity showed the closest match to the experimental results. The volume fraction of numerical simulations peaked as the wall was approached. The hydrodynamics of a pilot-scale CB FSB was simulated in order to predict the range of water flow to avoid the silica sand overflowing. The numerical simulations were in agreement with the experimental results qualitatively and quantitatively, and thus can be used to study the hydrodynamics of solid-liquid multiphase flow in CB FSB, which is of importance to the design, optimization, and amplification of CB FSBs.

**Key words** aquaculture; water recirculating; fluidized sand bed; hydrodynamics; numerical simulation; multiphase flow

## 1 Introduction

Rapid population growth and urbanization pose increasing challenge to the environment, including water quality. Biofilters are commonly used, in conjunction with other measures, in urban waste treatment facilities. Fluidized sand bed (FSB) is one of these biofilters that rely on a sand surface to absorb microbes in waste water. Compared to other filters, FSB is less costy and smaller in size (Weaver, 2006; Timmons *et al*., 2000), making it a favorite choice for recirculating aquaculture systems (Heinen *et al*., 1996). In recent years, FSBs are also being increasingly applied to industrial and municipal wastewater treatment facilities in China (Xu, 2006; Wang, 2006). A majority of these treatment projects focus on denitrification under anoxic conditions, different from aerobic nitrification in aquaculture.

The efficiency and behaviors of FSBs used in recirculating aquaculture systems have been examined in prior studies (Summerfelt, 2006; Davidson *et al*., 2008; Summerfelt and Cleasby, 1996; Summerfelt, 2006). For instance, Sánchez and Matsumoto (2012) have recently evaluated the organic matter, nitrogen and phosphorous removal efficiency of a physical and biological wastewater treatment system in an intensive Nile Tilapia laboratory recirculating production system. Cleasby (1990) studied the relationship among pressure drop, porosity and water velocity in fluidized-sand biofilters. Wen and Yu (1966) and Dharmarajah and Cleasby (1986) quantified the expansion of a clean sand bed for a given superficial water velocity under predefined conditions. More recently, the development of computer science and technology has introduced a combination of experiment, theory, and computational fluid dynamics (CFD) model simulation into FSB research. Vuthaluru *et al*. (2009) investigated the fluidization behavior of solid-liquid flow in a conical reactor using CFD modeling tools. Veerapen *et al*. (2005) proposed the methodology for designing swirl separators which are commonly used for removing solid wastes in recirculating aquaculture systems. Most of multiphase numerical simulations, however, were originally designed for certain chemical engineering problems (Reddy and Josh, 2009; He *et al*., 2012; Nikoo and Mahinpey, 2008; Panneerselvam *et al*., 2007), not necessarily suitable for the recirculating aquaculture systems. Few CFD studies have ever focused on the hydrodynamics of FSB in aquaculture. Such studies are challenging in nature due to the workload requirements to conduct such model simulations, as well as the lack of reliable laboratory data to verify the model performance.

* Corresponding author. Tel: 0086-532-82032522
E-mail: yuchuan@ouc.edu.cn

This study uses a three-dimensional, unsteady-state numerical model to study the hydrodynamics of lab-scale and pilot-scale CB FSB with three specific goals: 1) to estimate the relationship between bed expansion and water velocity; 2) to compare the influence of different drag models on simulations and then validate the simulations; and 3) to predict the hydrodynamics of the pilot-scale CB FSB. The size of a pilot-scale CB FSB was twice that of the lab-scale CB FSB in equal proportions. This study was developed for initial conditions without considering the density variation with time. However, particle density is an important controlling factor during the operation of FSBs. Biofilm growth increases the volume occupied by particles and reduces the effective density of the biofilm-coated sand, which in turn increases the bed volume and overall expansion of these particles (Summerfelt, 2006; Davidson, 2008). These factors need to be accounted for during this study.

## 2 Materials and Methods

### 2.1 Materials

Fig.1 shows the structure of a recirculating waste treatment system, and Table 1 shows the dimensions of the lab-scale CB FSB. Water is injected into an annular space (buffer pressure chamber) surrounding the base of a circular vessel. The water flowing continuously through the buffer pressure chamber generates strong rotation. A slot (rotating channel) is located at the base of the bed around the circumference of the vessel, and the water enters the FSB vessel through the slot. An inverted cone (rotating boss) is incorporated into the center of the floor of the vessel, which rotates the upward-flowing water.

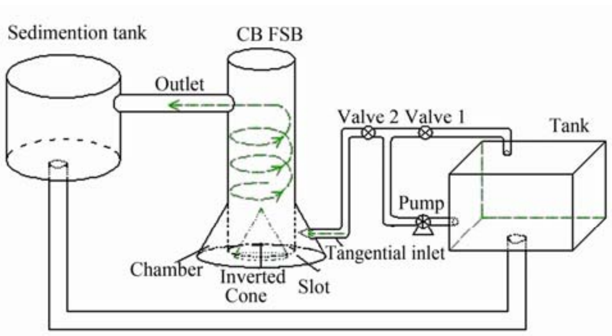


Fig.1 Schematic diagram of the recirculating system for synthetic aquaculture wastewater treatment.

Table1 Dimensions of lab-scale CB FSB

| Dimensions (mm) | Lab-scale CB FSB |
|---|---|
| Cylinder height | 1340 |
| Cylinder diameter | 190 |
| Cone height | 180 |
| Cone diameter | 170 |
| Chamber height | 60 |
| Chamber bottom diameter | 290 |
| Slot width | 1 |
| Inlet diameter | 20 |
| Outlet diameter | 100 |

The bed expansion is improved by the cone. At low flow rates, the quartz silica sand is static at the bottom of the vessel, and the water flows upward through pores without moving the sand. At higher flow rates, especially when the drag force of flowing fluid is greater than gravity, the particles are lifted and fluidization occurs. The dissolved waste in water is absorbed and transformed by microbes stuck on the surface of sand, provided that the residence time and quartz silica sand in the vessel are above certain thresholds.

### 2.2 Methods

The simulation result was consistent with actual problem needed to be ensured. However, the results of simulation were significantly influenced by the mesh of geometry, the CFD models, boundary conditions and material properties. Besides, simulation was applied to the structure optimization and industrialization amplification of CB FSB. Internal flow characteristics of CB FSB were changed by adjustment of structure parameters and alteration of size. The flow characteristics of CB FSB could be better understood by simulation. It provided theories for the structure optimization and application of CB FSB in industrial aquaculture.

#### 2.2.1 Simulation

#### 2.2.1.1 Computational geometry

The present study was carried out using the commercial CFD software FLUENT 6.3. First, the geometry was established and meshed to 20205 grids by tetrahedral-structured meshing technology using Gambit.

#### 2.2.1.2 CFD Model

The flow characteristics of solid-phase (silica sand) and liquid-phase (aquaculture wastewater) were studied in CB FSB. So the multiphase model was chosen. There are three kinds of multiphase model in FLUENT, namely, VOF Model, Mixture Model and Eulerian Model. VOF Model is suitable for stratified flow. Mixture Model and Eulerian Model are suitable for the problem where volume fraction of particles is more than 10%. The former is suitable for wide distribution of dispersed particles and the latter for concentrating distribution. The filling rate of silica sand was 31% in CB FSB. There was a clear separatrix in CB FSB after fluidization and silica sand was intensively distributed below the separatrix. So Eulerian Model was chosen as the multiphase model in this study. The water was in turbulent state in CB FSB. And only the $k$-$\varepsilon$ model was adopted in turbulent flow calculation of Eulerian Model. So $k$-$\varepsilon$ model was chosen as turbulence model. Besides, there were several forces on particle. Because the difference of density between solid and liquid was great, some forces were neglected, such as virtual mass force, Besset force and Magnus force. However, drag force was very important and can't be neglected at any time. So the choice of drag force model had significant influence on simulation.

## Eulerian Modeling

The CFD Eulerian multiphase modeling includes the Eulerian-Lagrangian and Eulerian-Eulerian approaches. The fluid flow is described by continuum equations, and the particulate phase flow is described by tracking the motion of individual particles in the Eulerian-Lagrangian models. These models are normally limited to a relatively small number of particles because of computational limitations. Fluid and solid phases are treated as interpenetrating continuum phases in Eulerian-Eulerian continuum models, which are most commonly used in fluidized bed simulations (Ding and Gidaspow, 1990). In addition, Eulerian-Eulerian modes are more suitable for dense flow and a greater number of particles. Therefore, the Eulerian multiphase modeling approach is used in the present study (Vuthaluru *et al*., 2009). The equations of continuity and momentum balance are shown below (Jiang and Huang, 2008).

The continuity equation of $q$ phase is expressed as follows:

$$\frac{\partial}{\partial t}(\alpha_q \rho_q) + \nabla.(\alpha_q \rho_q \vec{v}_q) = \sum_{p=1}^{n} \dot{m}_{pq} \ , \qquad (1)$$

where $\alpha_q$ is the volume fraction, $\rho_q$ is the density, $\vec{v}_q$ is the velocity, and $\dot{m}_{pq}$ is the mass transfer from $p$ phase to $q$ phase, and $t$ is time.

The momentum balance equation of $q$ phase is expressed as follows:

$$\frac{\partial}{\partial t}\left(\alpha_q \rho_q \vec{v}_q\right) + \nabla \cdot \left(\alpha_q \rho_q \vec{v}_q \vec{v}_q\right) = -\alpha_q \nabla p + \nabla \cdot \bar{\bar{\tau}}_q +$$

$$\alpha_q \rho_q \left(\vec{F}_q + \vec{F}_{\text{lift},q} + \vec{F}_{vm,\text{q}}\right) + \sum_{p=1}^{n}\left[\overline{R}_{pq} + \dot{m}_{pq}\vec{v}_{pq}\right], \qquad (2)$$

where $\vec{F}_q$ is the external volume force, $\vec{F}_{\text{lift},q}$ is the lift force,

$$\vec{F}_{\text{lift}} = -0.05 \rho_q \alpha_p \left|\vec{v}_q - \vec{v}_p\right| \times \left(\nabla \times \vec{v}_q\right),$$

$\vec{F}_{vm,q}$ is the virtual mass force,

$$\vec{F}_{vm} = 0.5 \alpha_p \rho_q \left(\frac{\mathrm{d}q v_q}{\mathrm{d}t} - \frac{\mathrm{d}p v_p}{\mathrm{d}t}\right),$$

$\overline{R}_{pq}$ is the mutual interaction of phases, $p$ is the presser of all phases, $\vec{v}_{pq}$ is the velocity of interphase, and $\bar{\bar{\tau}}_q$ is the stress-strain tensor.

## Turbulence Models

The $k$-$\varepsilon$ turbulence model has wide applicability and reasonable calculation accuracy. Especially, the RNG $k$-$\varepsilon$ turbulence model has higher reliability and calculation accuracy than standard $k$-$\varepsilon$ turbulence model. So the RNG $k$-$\varepsilon$ turbulence model was chosen in this study. The governing equations for the turbulent kinetic energy ($k$) and the energy dissipation rate ($\varepsilon$) are given by:

$$\frac{\partial}{\partial x}(\alpha_q \rho_q k_q) + \nabla \cdot (\alpha_q \rho_q \overrightarrow{\mathrm{U}}_q k_q) = \nabla \cdot (\alpha_q \frac{\mu_{t,q}}{\sigma_\kappa} \nabla k_q) +$$

$$\alpha_q G_{k,q} - \alpha_q \rho_q \varepsilon_q + \alpha_q \rho_q \prod_{kq} \text{, and}$$

$$\frac{\partial}{\partial x}(\alpha_q \rho_q \varepsilon_q) + \nabla \cdot (\alpha_q \rho_q \overrightarrow{\mathrm{U}_q} \varepsilon_q) = \nabla \cdot (\alpha_q \frac{\mu_{t,q}}{\sigma k} \nabla \varepsilon_q) +$$

$$\alpha_q \frac{\varepsilon_q}{k_q}(C_{1\varepsilon} \mathrm{G}_{k,q} - C_{2\varepsilon} \rho_q \varepsilon_q) + \alpha_q \rho_q \prod \varepsilon_q \ ,$$

where, $k_q$ is the turbulence kinetic energy of $q$ phase, $\overline{U_q}$ is the phase weighted velocity, $\varepsilon_q$ is the dissipation rate, $\prod k_q$ and $\prod \varepsilon_q$ are the influence of dispersed phase to continuous $q$ phase, $G_{k,q}$ is the generation of turbulence kinetic energy, $C$ is the constant, $\mu_{t,q}$ is the turbulent viscosity, its formula is:

$$\mu_{t,q} = \rho_q C_\mu \frac{k_q^2}{\epsilon_q} \ .$$

## Drag Force Models

There are several kinds of force acting on particles in CB FSB. Comparing with others, drag force is more important and is not ignorable. So the selection of drag models is important to the simulation. It is necessary to determine which model is most suitable for solid-liquid multiphase flow in CB FSB. Yasuna *et al*. (1995) showed that the solution of their model was sensitive to the value of drag coefficients. Enwald *et al*. (1996) found that the predictions based on different drag models concur with one another for dilute flow, but differ for dense flow. The solid-liquid flow involved in the present study belonged to the dense flow, and the influence of drag models on the simulation results was applied. Below are the solid-liquid transmit coefficients of different drag models (Jiang and Huang, 2008):

1) Syamlal-O'Brien (1989) model (SO):

$$K_{sl} = \frac{3\alpha_s \alpha_l \rho_l}{4 v_{r,s}^2 d_s} C_D \left(\frac{\mathrm{Re}_s}{v_{r,s}}\right) \left|\vec{v}_s - \vec{v}_l\right| ,$$

where $C_D = \left(0.63 + \frac{4.8}{\sqrt{\mathrm{Re}_s / v_{r,s}}}\right)^2$.

$l$ is the liquid phase, $s$ is the solid phase, $\alpha$ is the volume fraction, Re is the Reynolds number, $v$ is the velocity, $K_{sl}$ is the interphase exchange coefficient, and $C_D$ is the drag coefficient.

This model is suitable for conditions where the shear stress of solid phase is defined as Syamlal.

2) Wen and Yu (1966) model (Wen-Yu):

$$K_{sl} = \frac{3}{4} C_D \frac{\alpha_s \alpha_l \rho_l \left|\vec{v}_s - \vec{v}_l\right|}{d_s} \alpha_l^{-2.65},$$

where $C_D = \frac{24}{\alpha_l \mathrm{Re}_s}\left[1 + 0.15\left(\alpha_l \mathrm{Re}_s\right)^{0.687}\right]$.

This model is suitable for the dilute flow.

3) Gidaspow (1994) model (Gid):

For $\alpha_l > 0.8$, $K_{sl} = \frac{3}{4} C_D \frac{\alpha_s \alpha_l \rho_l \left|\vec{v}_s - \vec{v}_l\right|}{d_s} \alpha_l^{-2.65}$.

For $\alpha_l \le 0.8$, $K_{sl} = 150 \frac{\alpha_s (1-\alpha_l) \mu_l}{\alpha_l d_s} +$

$$1.75 \frac{\rho_l \alpha_s \left|\vec{v}_s - \vec{v}_l\right|}{d_s},$$

where $C_D = \frac{24}{\alpha_l \mathrm{Re}_s}\left[1 + 0.15\left(\alpha_l \mathrm{Re}_s\right)^{0.687}\right]$,

and $\mathrm{Re}_s = \frac{d_p V_s \rho_L}{\mu_L}$.

This model is suitable for the dense flow.

Drag Coefficient (DC) had significant influence on simulation, which was combined with granular viscosity (GV). In the following simulations, 4 different conditions were set, *i.e.*, DC = Gid, GV = SO; DC = Gid, GV = Gid; DC = SO, GV = SO; and DC = Wen-Yu, GV = SO. The closest match was chosen as the basic set in the following simulation by validation of experience.

### 2.2.1.3 Boundary conditions

The influent flow was unsteady, with no slip boundary condition employed at all walls. All terms of the governing equations for unsteady state were discretized using the first-order upwind differencing scheme. In all simulations, the time step of $1 \times 10^{-3}$ s was taken in the first 30 s, and the time step of $1 \times 10^{-2}$ s was used for the rest of time. The SIMPLE algorithm was employed for pressure-velocity coupling. The convergence criterion was set at $1 \times 10^{-3}$ for all the equations. The simulations were performed using a 64-bit machine with one processor having a clock speed of 2.4 GHz and 2 GB RAM on lab-scale and pilot-scale solid-liquid fluidized beds. CFD simulations were used to predict the velocity, volume fraction, and the track. The key parameters used in simulations are presented in Table 2.

Table 2 Key parameters used in simulations

| Description | Value | Comment |
|---|---|---|
| Particle density | 2600 kg m$^{-3}$ | Silica sand |
| Fluid density | 998.2 kg m$^{-3}$ | Water-liquid |
| Lateral boundary condition type | Wall | No-slip boundary condition |
| Inlet boundary condition type | Velocity at inlet | Superficial fluid velocity |
| Outlet boundary condition type | Outflow | Fully developed flow |
| Granular bulk viscosity | Lun *et al.* | Default in Fluent |
| Frictional viscosity | None | Default in Fluent |
| Granular temperature | Algebraic | Default in Fluent |
| Solids pressure | Lun *et al.* | Default in Fluent |
| Radial distribution | Lun *et al.* | Default in Fluent |
| Elasticity modulus | Derived | Default in Fluent |
| Packing limit | 0.6 | Fixed value |

### 2.2.2 Experiments

**Flow rate**

A bucket with a certain volume was filled with discharge flow. Time was recorded three times to obtain the average flow value. The 6 flow rates (14.51, 19.41, 26.94, 33.16, 45.97, 60.85 L min$^{-1}$) and their corresponding fluidized heights were measured.

**Diameter of silica sand**

In the experiment, filter sands were typically presieved to produce a distinct size ranging from 0.3 mm to 0.6 mm. Silica sand was chosen as the experiment material. Its density and viscosity were known. However, its diameter couldn't be decided. Silica sand was of different particle sizes within a certain range in experiment, whereas in the corresponding simulation, the diameter was set as mono-value. The diameter of sand in simulation must be identified first. So in the range of 0.3–0.6 mm in experiment, the diameter of sand was set 0.35, 0.45 and 0.55 mm in simulation. The closest match was chosen as the basic set in the following simulation by validation of experience.

### 2.2.3 Up-scaling theory

The final purpose of study about hydrodynamics of lab-scale is application of CB FSB in industrial aquaculture. However, the internal flow characteristics change in amplification. These changes can be well understood by simulation, which provides the theoretical basis for application of CB FSB in industrial aquaculture.

Bed expansion and fluid velocity in the experiment were influenced by the cone's flare angle, distance to wall, and the width of the slot. When the ratio of flare angle, distance to wall, and the width of the slot are kept constant, fluidization dynamics in an up-scaled CB FSB should be similar to that in experiment (Vuthaluru *et al.*, 2009). Pilot-scale CB FSB followed this up-scaling theory based on lab-scale CB FSB, implying twice the value with the principle of equilateral proportion of all parameters. Therefore, the pilot-scale CB FSB was simulated based on the results of the lab-scale CB FSB.

### 2.2.4 Calculation formula

1) Bed expansion

$$B = (V_{\text{fluidized}} - V_{\text{static}})/V_{\text{static}} \times 100\% ,$$

where $B$ is bed expansion of CB FSB, $V_{\text{static}}$ is the volume of static filter material, $V_{\text{fluidized}}$ is the volume of filter material with fluidization.

2) Average absolute errors of bed expansion

$$|e|_{av} = |B_{\text{experiment}} - B_{\text{simulation}}| / B_{\text{experiment}} \times 100\%$$

where, $B_{\text{experiment}}$ is the measured value of bed expansion, $B_{\text{simulation}}$ is the simulation value of bed expansion.

## 3 Results and Discussion

The hydrodynamic behavior of CB FSB varies with vessel dimensions, particle loading, and water flow rate. To understand the fluidization characteristics of the present system, we carried out systematic experiments from the following aspects: 1) to preliminarily study the hydrodynamics of lab-scale CB FSB through simulation; 2) to verify the reliability of simulations with experimental measurements; 3) to understand the regularity of particle distribution in CB FSB by volume concentration; and 4) to study the hydrodynamics of pilot-scale CB FSB based on the up-scale theory, further predicting the range of flow rate.

### 3.1 Bed Expansion for Lab-Scale CB FSB

In this section we investigate the effect of inflow velocity and silica sand size on the bed expansion of lab-scale CB FSB. In all the simulations the Eulerian model is used as a two-phase flow model, the RNG $k$-$\varepsilon$ model as a turbulence model, the Gidaspow correlation as a drag coefficient model, and the Syamlal-O'Brien correlation as kinetic granular viscosity (Vuthaluru *et al.*, 2009).

The bed expansion of lab-scale CB FSB was examined from three aspects. First, an example of flow regime evolution and the contours of fraction volume are shown in Fig.2. According to the contours of the fraction volume, the static height and fluidized height were obtained and further used for estimating the bed expansion. Next, Fig.3 shows that the bed size expands linearly with the inflow rate of water, in agreement with the experimental results of Summerfelt (2006). The correlation of bed expansion and time is shown in Fig.4. Due to different parameters used in each set, the stabilization time varied from 5 to 7 min. After the 7th minute, the flow dynamics reached a stabilized status. Thus, each set of simulation was carried out from the 8th minute, different from the setting in the study by Vuthaluru *et al.* (2009), *i.e.*, 4 min. The differences in the stabilization time are likely resulting from different mechanisms of flow injection, the sizes of the two set-ups, and the parameters in the simulation.

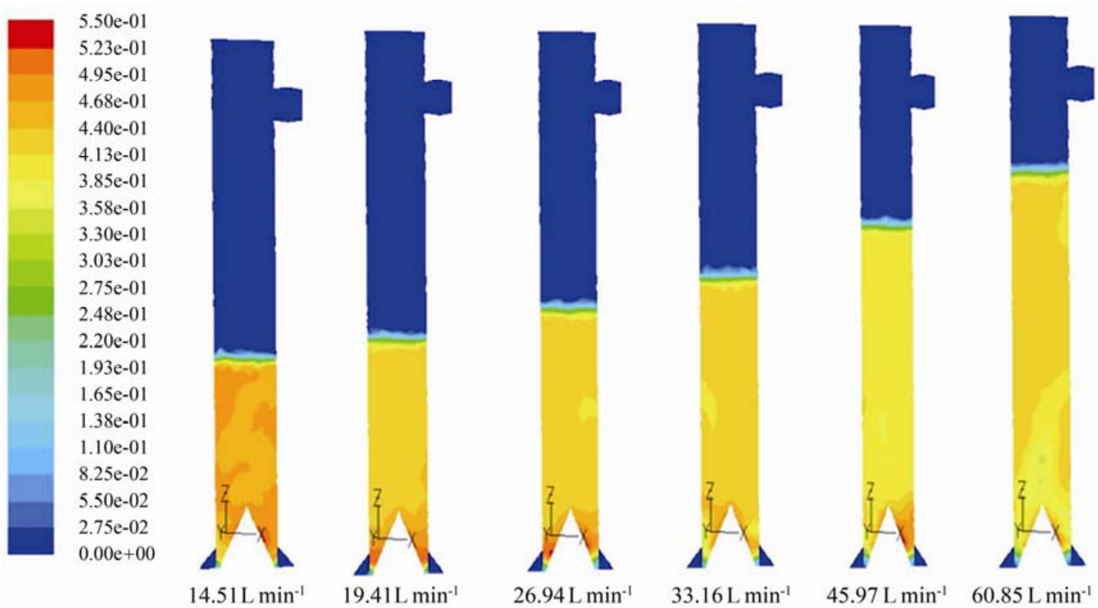

Fig.2 Contours of volume fraction in simulations at various inflow rates of water at the 8th min for 420 mm static height with 0.55 mm particles.

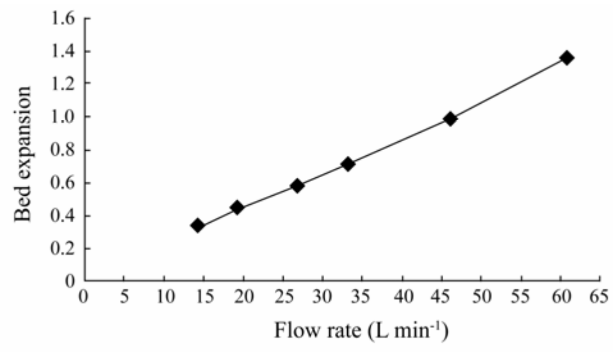


Fig.3 Bed expansion for lab-scale CB FSB with 420 mm static height, 0.55 mm particles.

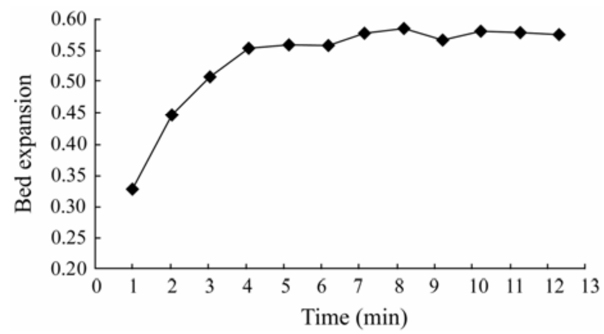


Fig.4 Bed expansion as a function of time for lab-scale CB FSB with a flow rate 26.94 L min$^{-1}$, 420 mm static height, 0.55 mm particles.

Fig.5 describes the bed expansion of different silica sand sizes. The bed expansion of 0.35 mm silica sand is greater than that of the 0.55 mm silica sand at the same water velocity, since smaller particles require less upward force lifting. For simulations using 0.35 mm silica sand, some of the silica sand particles overflow at the outlet pipe when water inflow rate is equal to or greater than 60.85 L min$^{-1}$, which is undesirable in industrial applications (Fig.6). These results indicate that finer particles require smaller water velocity to achieve the same bed expansion under the same condition. Finer particles also require less energy consumption. For example, when sand with $D_{10}$ > 0.4 mm is used in a FSB, the superficial water velocity required to maintain the bed expansion is possibly 2–4 times greater than that required for finer sand (Tsukuda *et al*., 1997). However, various factors including the treatment efficiency of wastewater, energy consumption, and overflow should be considered when selecting sand size in aquaculture. A previous study (Davidson *et al*., 2008) showed that the removal efficiency of carbonaceous biochemical oxygen demand ($cBOD_5$), total-ammonia-nitrogen (TAN), nitrite, and the dissolved oxygen consumption across the biofilter with 0.11 mm sand were obviously greater than that of 0.19 mm biofilter sand. The conclusion was that finer sand increased the difficulty in controlling bed expansion and the possibility of the sand to contact fish gills (Summerfelt, 2006), further causing harm and death to aquatic species such as fish.

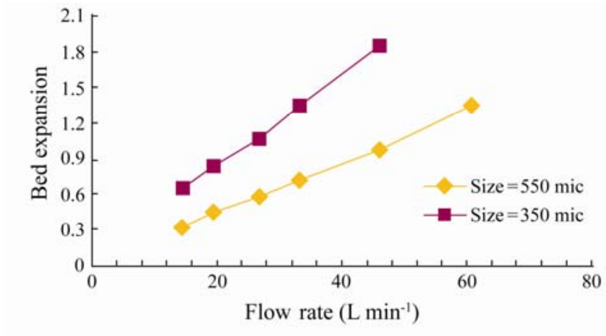


Fig.5 Comparison of bed expansion for different particle sizes for lab-scale CB FSB with 420 mm static height.

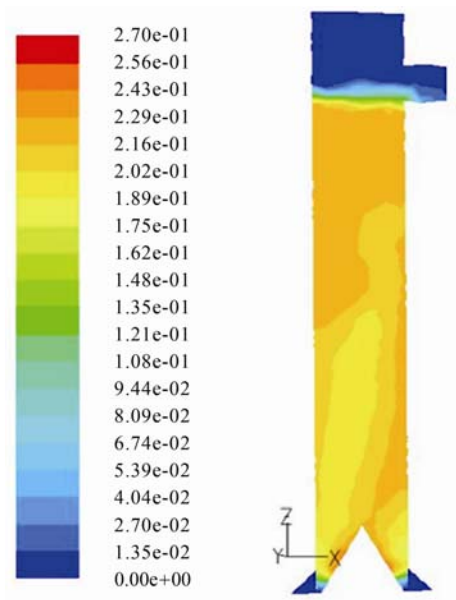


Fig.6 Silica sand overflow (flow rate 60.85 L min$^{-1}$; 0.35 mm particle size; 420 mm static height).

## 3.2 Validation of Lab-Scale CB FSB Simulations with Experimental Data

To validate the lab-scale CB FSB simulations, fluidized height and bed expansion were measured at six different velocities with a static height 420 mm in lab-scale CB FSB. In the experiment, silica sand was of different particle sizes within a certain range, whereas in the corresponding simulation, the diameter of silica sand was set as mono-value. The diameter of sand particles in simulation must be identified first.

The relationship of bed expansion and fluidized height changing with water flow is shown in Fig.7a. In both the simulations and experiments, bed expansion and fluidized height increase with the increases in flow rate and the diameter of silica sand. The simulations used the Gidaspow correlation for drag model and the Syamlal-O'Brien correlation for granular kinetic viscosity. The bed expansion average absolute errors, $|e|_{av}$ for 0.35, 0.45, and 0.55 mm models, compared with those in the experiment, were 0.6592, 0.2973, and 0.1653, respectively (Fig.7b). As 0.55 mm simulations gave the closest match, this particle size is used in the following simulations.

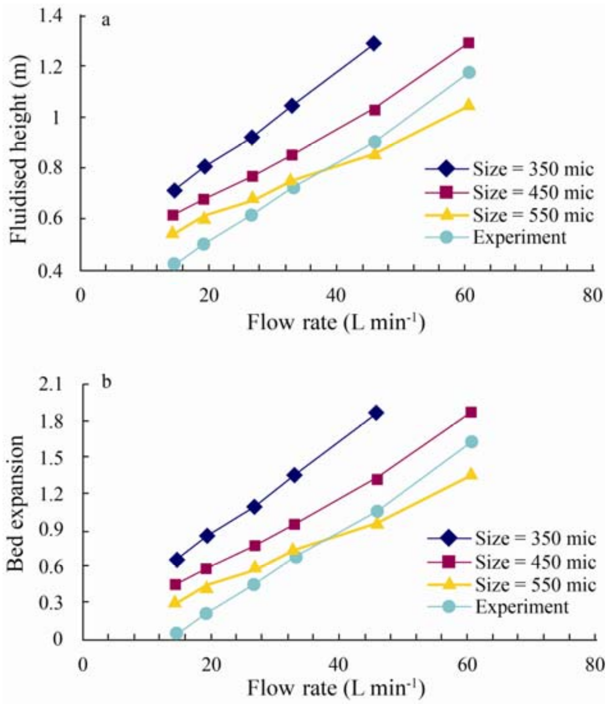


Fig.7 Comparison of experimental and several model simulations for deferent particle sizes for lab-scale CB FSB with 420 mm static height. a, fluidized height; b, bed expansion.

The influences of different drag coefficient models and granular kinetic viscosity on simulation results are shown in Fig.8. In the following simulations, 4 different combinations were set, *i.e.*, DC = Gid, GV = SO; DC = Gid, GV = Gid; DC = SO, GV = SO; and DC = Wen-Yu, GV = SO. Consequently, the bed expansion and fluidized height increased with an increasing flow rate in simulations and experiments. The error $|e|_{av}$ of bed expansion in the 4 sets of combinations compared in the experiment were 0.1653, 0.185, 0.1791, and 0.1906, respectively. As the simulation of DC = Gid and GV = SO gave the closest match, this model was used as a basis for the other simulations. The result suggests that different drag models influence the simulation in terms of the dense flow. However, there were no significant differences, in line with the results of the CFD modeling of a liquid-solid fluidized bed (Cornelissen *et al*., 2007) and the CFD modeling of fluidized limestone reactors for remediation of acidic drainage waters (Vuthaluru *et al*., 2009).

In addition, the bed expansion and fluidized height at a lower flow rate were smaller in the experiment than in the simulation, and the opposite was true for a higher flow rate. This phenomenon concurred with the study of Vuthaluru *et al*. (2009). The water inflow rates likely increased continuously, preventing the fluidized aggregate from settling down first in experiments. For the simulations, each set of a particular flow rate was initialized by an assigned static volume. In the experiments, previous fluidized aggregate might overestimate the fluidized height for a higher flow rate. Another possible reason inferred by Vuthaluru *et al*. (2009) is that the attrition of limestone particles is more apparent at higher flow rates than at lower rates, thereby producing finer particles with higher fluidized height. However, the silica sand used in the present work is harder than limestone, indicating that the abovementioned factors may not occur in short time.

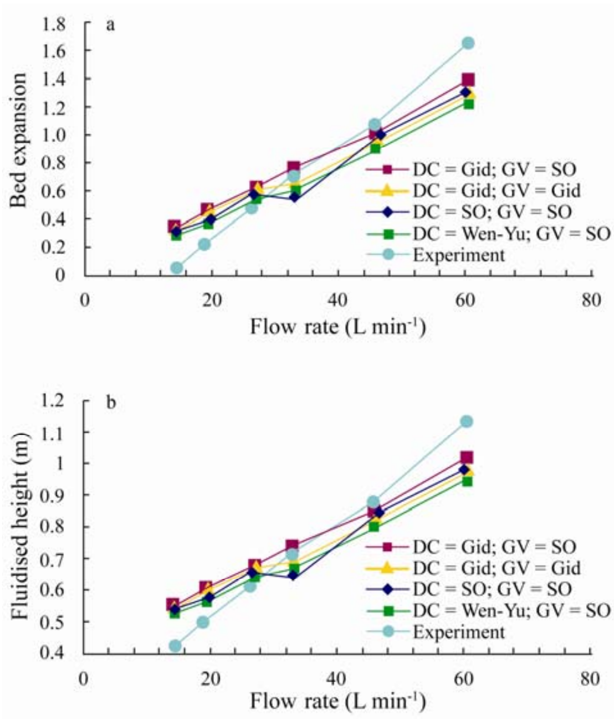


Fig.8 Comparison between experiments and several model simulations for different drag coefficient models and granular kinetic viscosity models for lab-scale CB FSB with 420 mm static height. a, fluidized height; b, bed expansion.

### 3.3 Analysis of Volume Concentration

The chosen cross section was parallel to the inflow pipe, and the diameter was equal to the diameter of CB FSB (Fig.9).

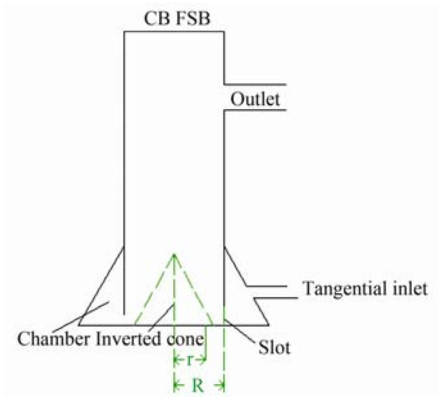


Fig.9 The cross section of lab-scale CB FSB.

The volume concentration of different sizes of silica sand through the same cross section in lab-scale CB FSB is shown in Fig.10a. The changes in radial volume concentration for three different particle sizes were basically the same, especially when the peaks of volume concentration appeared at about 5 cm of the radial direction, *i.e.*, r/R = 0.6. Centrifugal force likely decreased gradually in the radial direction, and the smaller force cannot transport particles to the wall at a certain distance from the base of the CB FSB. This trend was the same as that observed in the study of Cornelissen *et al*. (2007). However, the peak was different at r/R=0.8, possibly due to different injection mechanisms. In addition, the smaller the particle size, the smaller the volume concentration for silica sand of 3 different sizes. This was because the entrainment of turbulence overwhelmed more easily the centrifugal sedimentation for smaller particles. Therefore, the following of silica sand is better with water, and the bed expansion was larger. Furthermore, the per-unit volume of concentration becomes smaller. We conclude that the smaller the particles, the lesser the energy consumption.

The volume concentration of silica sand of the same size and the same cross section with different velocities in lab-scale CB FSB is shown in Fig.10b. The changes in radial volume concentration at 3 different velocities were similar, especially at the peaks of volume concentration. The velocity showed influences on the volume fraction. These results were slightly different from the result of Cornelissen *et al*. (2007), as the peak was more significant at higher flow than at lower flow with 3 mm beads. The possibility was that the size of silica sand was smaller at 0.55 mm, allowing the better following of silica sand with water.

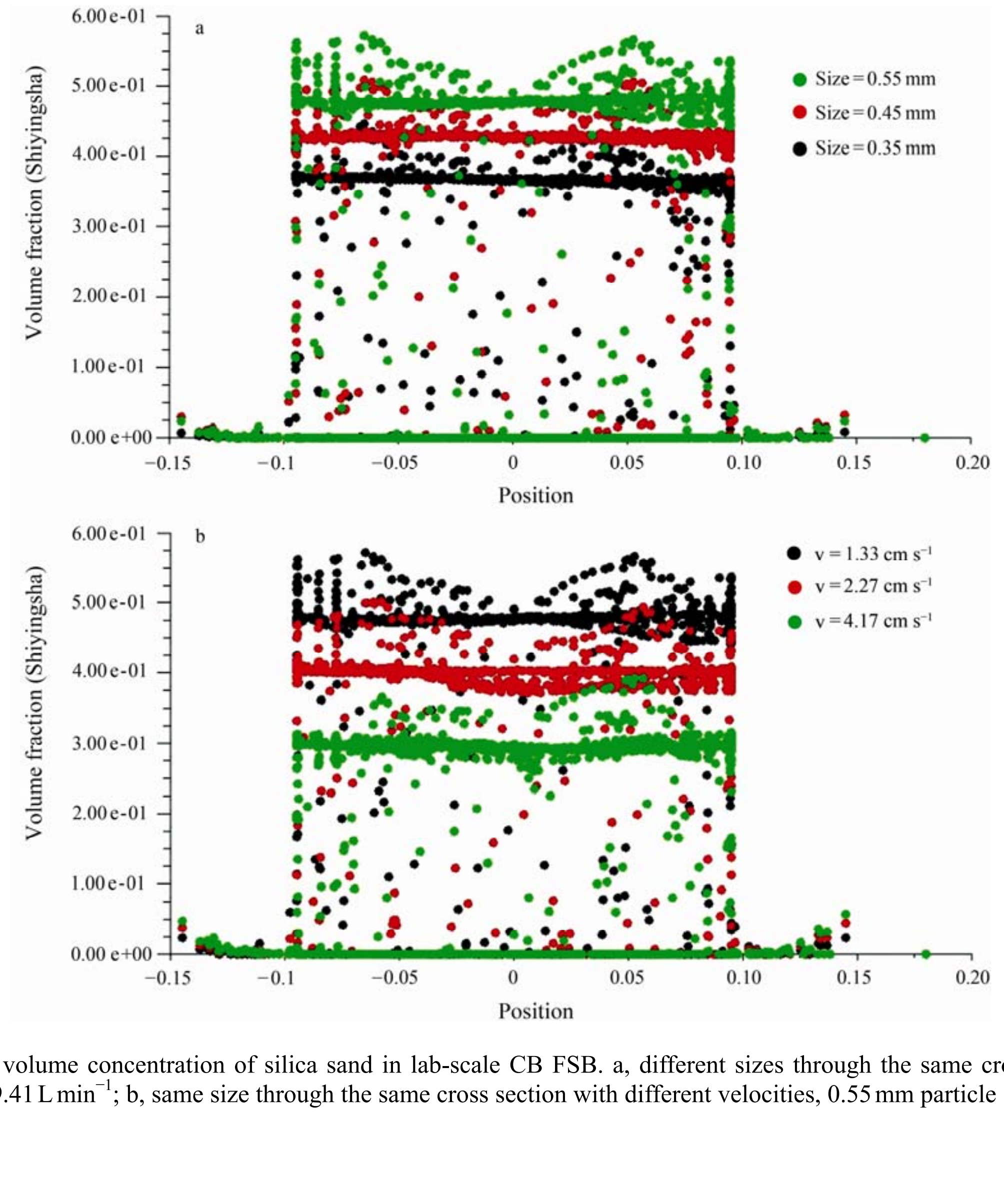


Fig.10 The volume concentration of silica sand in lab-scale CB FSB. a, different sizes through the same cross section, flow rate 19.41 L min$^{-1}$; b, same size through the same cross section with different velocities, 0.55 mm particle size.

### 3.4 Hydrodynamics of Pilot-scale CB FSB

Fig.11 shows that the bed expansion of the pilot-scale CB FSB increases with an increasing flow rate, similar to the observations in the lab-scale CB FSB. Summerfelt and Cleasby (1996) concluded that the $D_{90}$ fraction of the sand must expand at least 10% to 20% at the design superficial velocity in order to minimize the occurrence of static sand piles at the base of the bed. In addition, the $D_{10}$ fraction of sand must not expand excessively (*e.g.*, over 150%–200%) in order to prevent it from washing out the top of the FSB. Generally, an average clean-sand bed expansion is typically between 40% and 100% at a given superficial water velocity. The final expansion of FSB established with biofilm may reach 200%–300% (Summerfelt, 2006). The flow rate corresponding to the mean clean-sand bed expansion is called the design flow. Finally, FSB must be operated within a fairly narrow water flow range, *i.e.*, within about ±10%−30% of its design flow, to maintain proper bed expansion. Based on the combination in Fig.11, the bed expansions were set at 100%, and the design flow was at 150 L min$^{-1}$. In practice, the flow rate is controlled to be 105–195 L min$^{-1}$ for the pilot-scale CB FSB. However, the design, optimization, and amplification of CB FSB need a complete theory. Further study is needed to verify the optimal flow rate, especially when the actual environments vary in CB FSBs of different scales. Summerfelt (2004b) compared sand bed expansion measured in two scales of CB FSB and found that a given sand expanded roughly 10%–40% less in a full-scale CB FSB than that in a test column for the same hydraulic loading rate (Summerfelt *et al*., 2004b). The possibility was that there were small sand mounds because of the larger perimeter of the bed, storing a small volume of sand that was not fluidized. Considering the different actual environments in CB FSBs of various scales, we propose that large-scale CB FSBs should be produced for application of CFD to the design of a full-scale CB FSB.

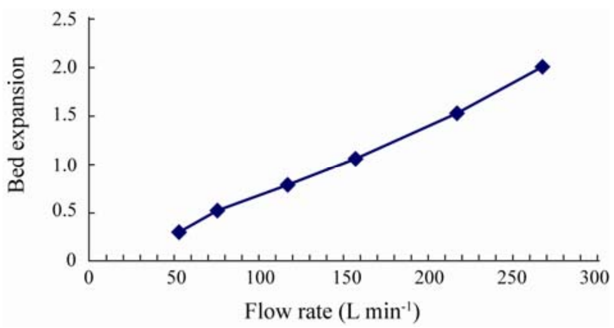


Fig.11 Bed expansion of pilot-scale CB FSB with 0.84 m static height.

## 4 Conclusions

This study employed a granular Eulerian turbulence model to investigate the dynamic characteristics of silica sand within the FSB. Lab-scale measurement data were used to evaluate the model predictions. The results of liquid-solid multiphase simulations of the CB FSB are summarized as follows:

1) Bed expansion increases with flow rate. At a fixed velocity, the smaller the particle size, the larger the bed expansion.

2) Through validation, the simulation involving 0.55 mm particles, the Gidaspow correlation for drag coefficient model, and the Syamlal-O'Brien correlation for kinetic granular viscosity closely match the experiment results, despite the errors between simulation and experimental results.

3) The peaks of volume concentration occurred at r/R = 0.6 under different conditions. These results show that higher bed expansion and better following of silica sand with water are attained when the particle size is smaller and the flow rate is higher.

4) The study on up-scale CB FSB hydrodynamics could predict the range of flow in practice by simulation for conducting the amplification of CB FSBs.

## Acknowledgements

This work was supported by the 12th Five-year National Technology Support Project (2011BAD13B04). The authors would like to thank Dr. Quansong Tong (Department of Marine, Earth and Atmospheric Sciences, North Carolina State University, Raleigh, USA) for improving the English in preparing the manuscript.

## References

Cleasby, J. L., 1990. Filtration. In: *Water Quality and Treatment. 4th ed*. Pontius, F. W., ed., American Water Works Association/McGraw-Hill, New York, 455-560.

Cornelissen, J. T., Taghipour, F., Escudiéa, R., Ellisa, N., and Grace, J. R., 2007. CFD modelling of a liquid-solid fluidized bed. *Chemical Engineering Science*, **62**: 6334-6348.

Davidson, J., Helwig, N., and Summerfelt, S. T., 2008. Fluidized sand biofilters used to remove ammonia, biochemical oxygen demand, total coliform bacteria, and suspended solids from an intensive aquaculture effluent. *Aquacultural Engineering*, **39**: 6-15.

Dharmarajah, A. H., and Cleasby, J. L., 1986. Predicting the expansion of filter media. *Water Works Association*, **78** (12): 66-76.

Ding, J., and Gidaspow, D., 1990. A bubbling fluidization model using kinetic theory of granular flow. *American Institute of Chemical Engineers Journal*, **36**: 523-538.

Enwald, H., Peirano, E., and Almstedt, A. E., 1996. Eulerian two-phase flow theory applied to fluidization. *International Journal of Multiphase Flow*, **22**: 21-66.

Gidaspow, D., 1994. *Multiphase Flow and Fluidization: Continuum and Kinetic Theory Descriptions*. Academic Press, San Diego, 467pp.

He, J., Göransson, K., Söderlind, U., and Zhang, W. N., 2012. Simulation of biomass gasification in a dual fluidized bed gasifier. *Biomass Conversion and Biorefinery*, **2**: 1-10.

Heinen, J. M., Hankins, J. A., and Weber, A. L., 1996. A semi-closed recirculating water system for high density culture of rainbow trout. *Progressive Fish Culturist*, **58**: 11-22.

Jayen, P. V., Brian, J. L., and Michel, F. C., 2005. Design methodology for the swirl separator. *Aquacultural Engineering*, **33**: 21-45.

Jiang, F., and Huang, P., 2008. *Advanced Application and Example Analysis of Fluent*. Tsinghua University Publishing House, Beijing, 328pp.

Nikoo, M. B., and Mahinpey, N., 2008. Simulation of biomass gasification in fluidized bed reactor using ASPEN PLUS. *Biomass Bioenergy*, **32** (12): 1245-1254.

Panneerselvam, R., Savithri, S., and Surender, G. D., 2007. CFD based investigations on hydrodynamics and energy dissipation due to solid motion in liquid fluidised bed. *Chemical Engineering Journal*, **132**: 159-171.

Reddy, R. K., and Joshi, J. B., 2009. CFD modeling of solid-liquid fluidized beds of mono and binary particle mixtures. *Chemical Engineering Science*, **64**: 3641-3658.

Sánchez, I. A., and Matsumoto, T., 2012. Hydrodynamic characterization and performance evaluation of an aerobic three phase airlift fluidized bed reactor in a recirculation aquaculture system for Nile Tilapia production. *Aquacultural Engineering*, **47**: 16-26.

Summerfelt, S. T., 2006. Design and management of conventional fluidized-sand biofilters. *Aquacultural Engineering*, **34**: 275-302.

Summerfelt, S. T., and Cleasby, J. L., 1996. A review of hydraulics in fluidized-bed biological filters. *Transactions of the American Society of Agricultural Engineers*, **39**: 1161-1173

Summerfelt, S. T., Davidson, J., and Helwig, N., 2004b. Evaluation of a full-scale CycloBio fluidized-sand biofilter in a coldwater recirculating system. In: *Proceedings of the Fifth International Conference on Recirculating Aquaculture*. Rakestraw, T. T., *et al*., eds., Virginia Polytechnic Institute and State University, Roanoke, VA, 227-237.

Syamlal, M., and O'Brien, T. J., 1989. Computer simulation of bubbles in a fluidized bed. *American Institute of Chemical Engineers Symposium Series*, **85**: 22-31.

Timmons, M. B., Helwig, N., and Summerfelt, S. T., 2000. The cyclone sand biofilter: A new design concept and field evaluation. In: *Proceedings of the Third International Conference on Recirculating Aquaculture*. Libey, G. S., and Timmons, M. B., eds., Virginia Polytechnic Institute and State University, Roanoke, VA, 222-226.

Tsukuda, S. M., Hankins, J. A., Marshall, C. P., Summerfelt, S. T., Bullock, G. L., and Sawyer, T. K., 1997. Effects of sand size on fluidized-bed biofilter performance in cold water systems. In: *Advances in Aquacultural Engineering*, *NRAES*-105. Timmons, M. B., and Losordo, T., eds., Northeast Regional Agricultural Engineering Service, Ithaca, New York, 368-380.

Veerapen, J. P., Lowry, B. J., and Couturier, M. F., 2005. Design methodology for the swirl separator. *Aquacultural Engineering*, **33**: 21-45

Vuthaluru, R., Tade, M., Vuthaluru, H., Tsvetnenkob, Y., Evansb, L., and Milne, J., 2009. Application of CFD modelling to investigate fluidized limestone reactors for the remediation of acidic drainage waters. *Chemical Engineering Journal*, **149**: 162-172.

Wang, Q., 2006. Treatment of phenols wastewater with biochemistry method. PhD thesis. Tianjin University.

Weaver, D. E., 2006. Design and operations of fine media fluidized bed biofilters for meeting oligotrophic water requirements. *Aquacultural Engineering*, **34**: 303-310.

Wen, C. Y., and Yu, Y. H., 1966. Mechanics of fluidization. In: *Chemical Engineering Progress Symposium Series* 62. American Institute of Chemical Engineers, New York, 153pp.

Xu, G. D., 2006. Study on the characteristics and applications of a sequential batch bi-external recycling biological fluidized bed. PhD thesis. Shanghai University.

Yasuna, J. A., Moyer, H. R., Elliott, S., and Sinclair, J. L., 1995. Quantitative predictions of gas-particle flow in a vertical pipe with particle-particle interactions. *Powder Technology*, **84**: 3-34.

**(Edited by Qiu Yantao)**